Ab Initio Studies of Exciton g Factors: Monolayer Transition Metal Dichalcogenides in Magnetic Fields

Thorsten Deilmann,* Peter Krüger, and Michael Rohlfing
Institut für Festkörpertheorie, Westfälische Wilhelms-Universität Münster, 48149 Münster, Germany

(Received 18 February 2020; accepted 15 May 2020; published 2 June 2020)

The effect of a magnetic field on the optical absorption in semiconductors has been measured experimentally and modeled theoretically for various systems in previous decades. We present a new first-principles approach to systematically determine the response of excitons to magnetic fields, i.e., exciton g factors. By utilizing the GW-Bethe-Salpeter equation methodology we show that g factors extracted from the Zeeman shift of electronic bands are strongly renormalized by many-body effects which we trace back to the extent of the excitons in reciprocal space. We apply our approach to monolayers of transition metal dichalcogenides (MoS_2, $MoSe_2$, $MoTe_2$, WS_2, and WSe_2) with strongly bound excitons for which g factors are weakened by about 30%.

DOI: 10.1103/PhysRevLett.124.226402

Introduction.—The response of a semiconductor to magnetic fields is intimately linked to its quantum mechanical properties. The two main effects, the Zeeman and the diamagnetic shift, have been employed by many researchers to study the electronic and optical properties of, e.g., bulk semiconductors [1,2], quantum dots [3,4], or recently atomically thin materials, e.g., two-dimensional transition metal dichalcogenides (TMDCs) [5–8]. The nature of the quantum mechanical states involved in optical processes (excitons, i.e., electron-hole pairs) determines its shift in the magnetic field, the so-called exciton g factor. Due to the unique character of each excitation, g factors allow for their identification and the analysis of their properties. E.g., interlayer excitons in bulk $MoTe_2$ have been discovered by the different sign of its g factor [9]. In TMDCs often a variety of exciton lines with different shifts are found with measured values of about -4, -8, or even stronger [10]. For higher excited Rydberg excitons $2s$, $3s$, etc. stronger g factors than for its $1s$ counterpart have been reported [11–13]. Changing values have also been observed in temperature and doping dependent measurements [14,15]. At present, however, a conclusive understanding and *ab initio* prediction of exciton g factors is still missing.

On a single particle level, the fundamental theory of semiconductors in magnetic fields has been formulated by Kohn [16] and Roth [17] around the 1960s. For the calculation of the magnetization, i.e., the $\mathbf{k}$-integrated magnetic moment, it has later been reformulated on the basis of the Berry phase, e.g., for ferromagnets [18–22]. Most theoretical descriptions to evaluate exciton g factors are based on models applying $\mathbf{k}\cdot\mathbf{p}$ theory [10,23–30]. Within these approaches, however, only the individual magnetic moments of *single* electrons and holes are considered while the *excitonic* many-body nature of the correlated electron-hole pair is typically ignored.

In this Letter, we present a new first-principles approach merging the evaluation of the $\mathbf{k}$-resolved orbital magnetic moments and the properties of the excitons to calculate its g factors. These calculations employ *ab initio* density functional theory (DFT) and the GW-Bethe-Salpeter equation (BSE) [31,32]. While the explicit use of magnetic fields is challenging in a self-consistent approach, it is certainly possible to utilize the wave functions to calculate band- and $\mathbf{k}$-dependent magnetic moments from perturbation theory. To this end, we rewrite the original approach [16,17] into the form of Chang *et al.* [18]. The resulting magnetic moments take into account the full Bloch states, i.e., the calculations are beyond a local approximation which treats only contributions from small spheres around the atoms. To evaluate exciton g factors we consider the spatial structure of the excitation gained from the BSE. After introducing our approach for $MoSe_2$, we discuss the results for the five well-known TMDC monolayers MoS_2, $MoSe_2$, $MoTe_2$, WS_2, and WSe_2 and compare them to experiment. We show that exciton g factors based on full Bloch states are enhanced with respect to those from the local approximation while they are weakened by their many-body character.

A quantum mechanical system in a homogeneous magnetic field [we use $\mathbf{B} = (0, 0, B_z)$ as in most experiments] is described by the effective one-particle Hamiltonian

$$\begin{aligned}\hat{H}^{\mathrm{eff}} &= \hat{H}_0^{\mathrm{eff}} + \frac{e}{2m_e}(\hat{L}_z + g_e\hat{S}_z)B_z + \frac{e^2}{2m_e}(x^2+y^2)B_z^2 \\ &=: \hat{H}_0^{\mathrm{eff}} - \hat{m}_z B_z + \mathcal{O}(B_z^2),\end{aligned} \tag{1}$$

where $\hat{H}_0^{\mathrm{eff}}|\Psi_{n\mathbf{k}}^0\rangle = E_{n\mathbf{k}}|\Psi_{n\mathbf{k}}^0\rangle$ is the nonperturbed DFT or GW Hamiltonian, respectively, including spin-orbit coupling. $\hat{L}_z$ and $\hat{S}_z$ are angular momentum and spin operator

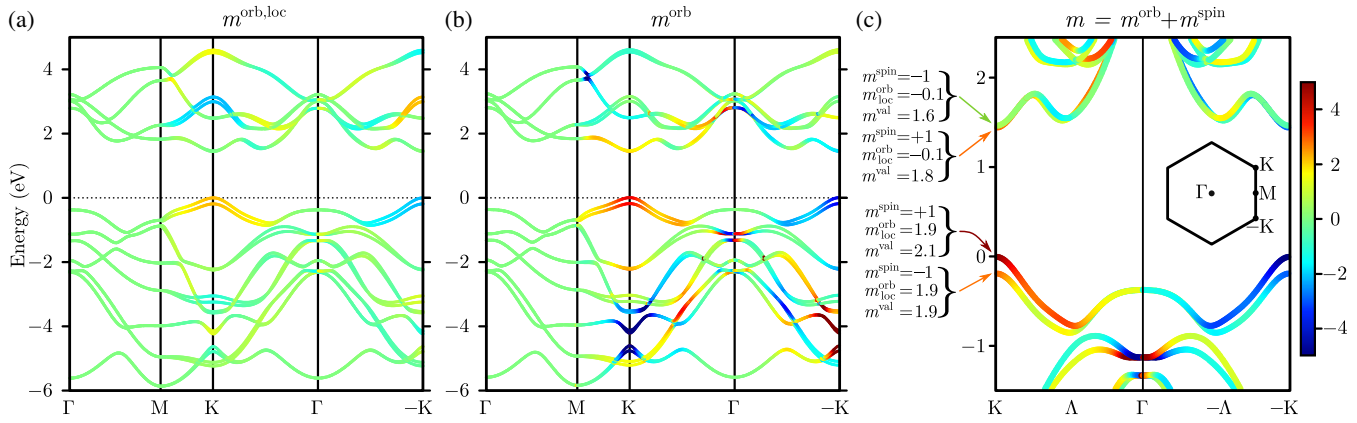

FIG. 1. DFT band structure of $MoSe_2$. In (a) the bands are colored according to the expectation values of the local orbital magnetic moments $m^{\mathrm{orb,loc}}_{n\mathbf{k}}$ [Eq. (3)]. In contrast to this, in (b) the orbital magnetic moment $m^{\mathrm{orb}}_{n\mathbf{k}}$ including the contribution from the Bloch states is shown [Eq. (5)]. The corresponding color scale is shown in units of μ_{B}. In (c) an enlargement along KΓ − K is shown in which the spin contributions have been added. The colors refer to the total magnetic moments $m_{n\mathbf{k}} = m^{\mathrm{orb}}_{n\mathbf{k}} + m^{\mathrm{spin}}_{n\mathbf{k}}$. On the left side we break down the different contributions of m at the K point (see main text).

and g_e is the free electron g factor. In this Letter, we will focus on the linear Zeeman term mB_z (we omit the index z for brevity) and neglect the diamagnetic term that is quadratic in B_z. The magnetic moment can be further divided into

$$\hat{m} =: \hat{m}^{\mathrm{orb}} + \hat{m}^{\mathrm{spin}} = -\frac{e}{2m_e}\hat{L} - \frac{eg_e}{2m_e}\hat{S}. \tag{2}$$

In the case of an isolated hydrogen atom these numbers correspond to the magnetic quantum number m_l and the spin quantum number m_s. In a periodic semiconductor its expectation value for band n at $\mathbf{k}$ can be calculated by $m_{n\mathbf{k}} = \langle \Psi^0_{n\mathbf{k}} | \hat{m}^{\mathrm{orb}} | \Psi^0_{n\mathbf{k}} \rangle + \langle \Psi^0_{n\mathbf{k}} | \hat{m}^{\mathrm{spin}} | \Psi^0_{n\mathbf{k}} \rangle$.

Magnetic moments of Bloch states.—While the calculation of the spin part in Eq. (2) is easy once the spinors are known, the evaluation of the orbital part is more delicate. The spatial dependency of the operator $\hat{L}_z = x\hat{p}_y - y\hat{p}_x$ prevents a straightforward calculation and we will discuss two different approaches: (i) the most simple way to tackle the problem is a local approximation as it has been carried out earlier for the magnetization [22,33]. Within this approximation, we can easily evaluate

$$m^{\mathrm{orb,loc}}_{n\mathbf{k}} = \langle \Psi_{n\mathbf{k}} | x\hat{p}_y - y\hat{p}_x | \Psi_{n\mathbf{k}} \rangle_{\mathrm{loc}} \tag{3}$$

in a basis of Gaussian orbitals [34] in a local sphere around each atom in the unit cell, yielding the data of Fig. 1(a). However, in regions of the Brillouin zone where the Berry curvature is large (see the Supplemental Material [35]) this approximation for the magnetic moments clearly fails [see Figs. 1(a) and 1(b)]. (ii) To account for the full Bloch states, i.e., considering the different contributions of $\hat{L}_z$ with the lattice-periodic wave function in different unit cells, we follow the approach proposed by Kohn [16] and Roth [17]

$$\bar{m}^{\mathrm{orb}}_{n\mathbf{k}} = -\frac{i\mu_{\mathrm{B}}}{m_e}\sum_{n'\neq n}\left(\frac{\langle u_{n\mathbf{k}}|\hat{p}_x|u_{n'\mathbf{k}}\rangle\langle u_{n'\mathbf{k}}|\hat{p}_y|u_{n\mathbf{k}}\rangle}{E_{n'\mathbf{k}} - E_{n\mathbf{k}}} - \frac{\langle u_{n\mathbf{k}}|\hat{p}_y|u_{n'\mathbf{k}}\rangle\langle u_{n'\mathbf{k}}|\hat{p}_x|u_{n\mathbf{k}}\rangle}{E_{n'\mathbf{k}} - E_{n\mathbf{k}}}\right). \tag{4}$$

By using the commutator relation $i[\hat{H}, x_j] = (\hbar/m_e)\hat{p}_{x_j}$ one can transform Eq. (4) to Eq. (5), which has been derived by Chang *et al.* [18] for the magnetic moment of a wave packet

$$m^{\mathrm{orb}}_{n\mathbf{k}} = \mu_{\mathrm{B}}\mathrm{Im}\left\langle \frac{\partial u_{n\mathbf{k}}}{\partial k_x}\middle| \hat{H}(\mathbf{k}) - E_{n\mathbf{k}} \middle| \frac{\partial u_{n\mathbf{k}}}{\partial k_y}\right\rangle. \tag{5}$$

Taking special care on the nonlocal pseudopotential [45,46], we find that both Eqs. (4) and (5) lead to equivalent magnetic moments at the ±K point if we consistently use DFT or *GW* energies, respectively, and the corresponding wave functions [47]. We note that the increased gap in *GW* [48,49] generally leads to larger magnetic moments. Due to the numerical stability [Eq. (4) diverges for degenerated states] we employ Eq. (5) in the following yielding the data of Fig. 1(b).

Magnetic moments of the bands in $MoSe_2$.—In a TMDC monolayer like, e.g., $MoSe_2$ each band consists of a superposition of different orbitals of different atoms. Close to the K point the character of the topmost valence bands is dominated by the Mo atoms with a contribution of more then 80% which stems from the d orbitals, whose major part of about 90% is related to the spherical harmonics $Y_{2,\pm 2}$ ($d_{x^2-y^2}$ and d_{xy} orbitals). The remaining 18% are shared by p_x and p_y orbitals of Se atoms. In contrast to this, the lowest conduction band is dominated by Mo $Y_{2,0}$ (d_{z^2} orbital) with a share of about 55%. In Fig. 1(a) the resulting

TABLE I. Magnetic moments from Eq. (5) (in μ_B) at the K point, their differences $g_{\text{band}}^{\text{"A/B"}}$ which resemble the main contribution of the bright A and B transitions [e.g., for MoS_2 $g_{\text{band}}^{\text{"A"}} = 2(m_{\text{CB,K}} - m_{\text{VB,K}})$ and $g_{\text{band}}^{\text{"B"}} = 2(m_{\text{CB+1,K}} - m_{\text{VB-1,K}})$], and resulting g factors from Eq. (7). In comparison several experimental measurements of the g factor of the A and B exciton are listed. Note that for our magnetic moments m we expect an error of about $\pm 0.05\mu_B$, as well as about ± 0.1 for the g factors.

Material	$m_{\text{VB}-1/\text{VB,K}}$	$m_{\text{CB/CB}+1,\text{K}}$	$g_{\text{band}}^{\text{"A/B"}}$	$g^{\text{A/B}}$	g^{A} (experiment)	g^{B} (experiment)
MoS_2	2.94/5.10	2.98/0.76	−4.24/ − 4.36	−3.06/ − 3.10	−1.7 [51], −3.0 [12], −3.8 [12], −4.0 [52], −4.2 [10], −4.6 [53]	−4.3 [53], −4.65 [52]
$MoSe_2$	2.81/5.03	2.74/0.46	−4.58/ − 4.70	−3.22/ − 3.28	−3.8 [54,55], −4.1 [5], −4.2 [10], −4.3 [12], −4.4 [53]	−4.2 [10]
$MoTe_2$	2.71/5.03	2.60/0.21	−4.86/ − 5.00	−3.36/ − 3.36	−4.6 [8,12]	−3.8 [8]
WS_2	3.29/5.94	1.35/4.21	−3.46/ − 3.88	−2.76/ − 2.80	−3.7 [10], −3.94 [52], −4.0 [12], −4.25 [56], −4.35 [57]	−3.99 [52], −4.9 [10]
WSe_2	3.15/5.91	0.99/3.97	−3.88/ − 4.32	−3.00/ − 3.22	−1.6.. − 2.9 [6], −3.2 [58], −3.7 [55], −3.8 [10], −4.37 [7]	−3.9 [10]

local magnetic moment [Eq. (3)] is shown. Indeed, as the discussion of the special harmonics suggests, we find a value of $m_{\text{VB,K}}^{\text{orb,loc}} = 1.93\mu_B$ for both spin-orbit split valence bands and of $m_{\text{CB,K}}^{\text{orb,loc}} = -0.09\mu_B$ for the conduction bands. Further away from the K point the moments almost vanish. At −K the sign of the orbital moment is exactly reversed. In general we find the orbital magnetic moments of $MoSe_2$ to be $-2 \leq m_{\text{loc}}^{\text{orb}} \leq 2$ for bands close to the Fermi level, which corresponds well to the s, p, and d wave function character. Note that, e.g., in the ΓM direction, the magnetic moments are zero even though strong p and d characters are observed, which underlines the importance of the relative phase of the contributing orbitals in the superposition.

However, this local approximation is oversimplified. In a periodic semiconductor the correct physical states are Bloch waves. Taking this into account [16,17] reveals several important quantitative differences [Fig. 1(b)]. While the orbital momentum at Γ remains zero, the situation at ±K is distinctly changed. For the valence bands we find slightly different values close to 4 while m^{orb} of the conduction bands is slightly smaller then $2\mu_B$ based on DFT. The difference to the local picture is given as the so-called valley contribution [10] $m^{\text{val}} = m^{\text{orb}} - m_{\text{loc}}^{\text{orb}} = 2.1$ and $1.8\mu_B$, respectively. When employing GW the deviations from the local approximation are even larger and we calculate $m^{\text{orb}} = 5.6$ and $3.2\mu_B$ ($m^{\text{val}} = 3.7$ and $3.3\mu_B$), respectively. If not noted explicitly, we will stick to the DFT results and refer to the Supplemental Material [35] for further discussion.

For calculating the entire magnetic moment the spin part is still missing. In Fig. 1(c) we show an enlargement with the bands colored according to $m_{n\mathbf{k}} = m_{n\mathbf{k}}^{\text{orb}} + m_{n\mathbf{k}}^{\text{spin}}$. At the ±K points the valence and conduction bands have opposite spin direction due to the spin-orbit interaction. Hence, at K the two topmost valence bands have a magnetic moment of about $m_{\text{VB,K}} = 2.8$ and $5.0\mu_B$, respectively. The same happens for the two lowest conduction bands which are close in energy ($m_{\text{CB,K}} = 2.7$ and $0.5\mu_B$). Also the spin part acts with a reversed sign at −K so that $m_{n,\text{K}} = -m_{n,-\text{K}}$ holds [50]. We observe similar but quantitatively different results for all TMDC monolayers. We will subsequently discuss and compare the numbers (see Table I).

Evaluation and interpretation of exciton g factors.—We now deduce the effects of a small magnetic field on *excitons*. In an oversimplified picture an exciton would be a transition from one point $\mathbf{k}$ in a valence band to another point $\mathbf{k} + \mathbf{Q}$ in a conduction band, and its change with the magnetic field would be given by the difference $m_{c\mathbf{k}+\mathbf{Q}} - m_{v\mathbf{k}}$. However, this approximation (which means neglecting the electron-hole interaction) is known to be unsatisfactory for most systems and, in particular, for 2D systems with large exciton binding energies [59]. The state-of-the-art approach to account for two-particle excitations is the BSE [31,32,60] which is given in the Tamm-Dancoff approximation by

$$(\epsilon_{c\mathbf{k}+\mathbf{Q}} - \epsilon_{v\mathbf{k}})A_{vc\mathbf{k}}^{(N,\mathbf{Q})} + \sum_{v'c'\mathbf{k}'} K_{vc\mathbf{k},v'c'\mathbf{k}'}(\mathbf{Q})A_{v'c'\mathbf{k}'}^{(N,\mathbf{Q})} = \Omega^{(N,\mathbf{Q})}A_{vc\mathbf{k}}^{(N,\mathbf{Q})}. \tag{6}$$

Here, $\Omega^{(N,\mathbf{Q})}$ is the energy of exciton N and $A_{vc\mathbf{k}}^{(N,\mathbf{Q})}$ its amplitudes, which contain the complete spatial structure. Again we assume moderate magnetic fields, i.e., that the change of electron-hole interaction $K_{vc\mathbf{k},v'c'\mathbf{k}'}(\mathbf{Q})$ due to the field can be neglected. Consequently, the influence of a magnetic field on the energy of an exciton is given by the field induced change of the band structure energy differences $\epsilon_{c\mathbf{k}+\mathbf{Q}} - \epsilon_{v\mathbf{k}}$ of all contributing transitions. We can eventually evaluate the effective exciton g factor of the exciton N with momentum $\mathbf{Q}$ by

$$g^{(N,\mathbf{Q})} = 2\sum_{vc\mathbf{k}} |A_{vc\mathbf{k}}^{(N,\mathbf{Q})}|^2 (m_{c\mathbf{k}+\mathbf{Q}} - m_{v\mathbf{k}})/\mu_B. \tag{7}$$

In experiment (effective) g factors are typically defined on the basis of the energy difference between measurements

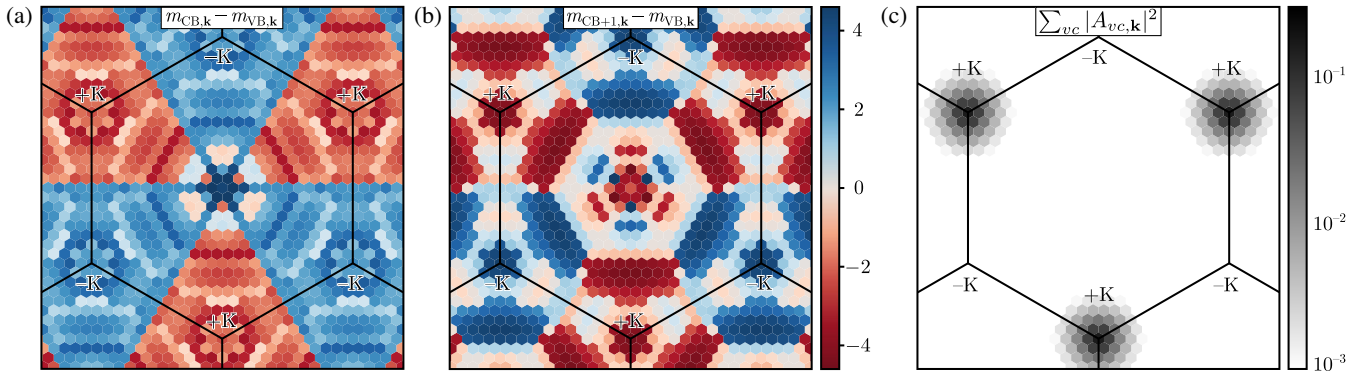

FIG. 2. (a),(b) Difference of the magnetic moments of $MoSe_2$'s first and second conduction band (CB, CB + 1, respectively) and the valence band (VB). The results are shown on a (24×24) mesh with colors from red to blue denoting the differences. Note that the abrupt changes (e.g., red to blue) are related to band crossings. (c) k-dependent exciton wave function of the first bright (A) exciton on a logarithmic scale. Note that due to the magnetic field the ±K degeneracy is lifted. The resulting exciton g factor is calculated by multiplying the magnetic moments with the exciton wave functions [see Eq. (7)].

with right- and left-handed circular polarized light $g\mu_B B_z := \Omega_{\sigma^+} - \Omega_{\sigma^-}$ [52]. This results in the factor 2 in Eq. (7). If excitonic effects were neglected, the g factor of the transition from $(v,\ \mathbf{k})$ to $(c,\ \mathbf{k}+\mathbf{Q})$ could be approximated by

$$g_{\mathrm{band}}^{(v\mathbf{k}\to c\mathbf{k}+\mathbf{Q})} = 2(m_{c\mathbf{k}+\mathbf{Q}} - m_{v\mathbf{k}})/\mu_B. \tag{8}$$

Equation (7) is a generalization of g_{band}. Our results show that g is more than 30% smaller compared to g_{band} due to the spatial structure of the excitons.

Exciton g factors of $MoSe_2$.—Using Eq. (7) we are now able to calculate the energy splitting of excitons in a magnetic field, i.e., its g factors. In Figs. 2(a) and 2(b) the resulting differences of the magnetic moments between the valence band and the first and second conduction bands are shown. These differences are weighted in Eq. (7) by the square of the exciton wave function, which is shown on a logarithmic scale in Fig. 2(c) for the case of the exciton at K. In Mo-based TMDCs the exciton transition to the lowest conduction band is *bright* due to the same spin character [61,62], i.e., the so-called A exciton. We find that the interband transition exactly at K involves a change of the magnetic moment of $-2.3\,\mu_B$ while at −K the moment is reversed, which would yield $g_{\mathrm{band}}^{\mathrm{A}} = 2(-2.3) = -4.6$. Away from ±K the absolute value of the magnetic moment decreases (see [35] for details) and if we take the $\mathbf{k}$ space dependent structure into account we find a distinctly weaker g^{A} factor of −3.2. The second excited Rydberg state is considerably more extended in real space and hence more localized in reciprocal space. Consequently $g^{\mathrm{A}^{2s}} = -3.7$ is much stronger, even though stemming from the same bands [11]. In the following we refer our wording to the absolute values of the g factor. The transition to the second conduction band (VB + 1) is the first *dark* transition. In Fig. 2(b) the calculated magnetic moments are shown. Here, we find a distinctly larger difference of the magnetic moments of $-4.6\mu_B$ at K and a decrease close to K as discussed before. The weighted sum amounts to $g^{\mathrm{D}} = -7.4$ (compared to $g_{\mathrm{band}}^{\mathrm{D}} = 2(-4.6) = -9.2$). Besides momentum direct excitons discussed before, we can also use Eq. (7) to evaluate indirect excitons [63]. We find, e.g., for the lowest energy transitions $g = 12.0$ ($g_{\mathrm{band}} = 15.6$) for $\mathrm{K} \to \mathrm{K}'$ and $g = -6.0$ ($g_{\mathrm{band}} = -8.6$) for $\mathrm{K} \to \Lambda$.

Comparison of different TMDCs.—Table I compiles our data of all five TMDC monolayers studied here. We first focus on the difference of the transition exactly at K. Changing the chalcogen atom from S to Se and further to Te leads to an increase in $g_{\mathrm{band}}^{\mathrm{A}}$. E.g., for Mo the value changes from −4.3, to −4.6 and −4.9, respectively. If the metal atom is tungsten, the magnetic moments are smaller and we find −3.5 and −3.9. The transition from the second highest valence band (VB-1) at K (corresponding to the B exciton), results in a very similar trend. However, compared to $g_{\mathrm{band}}^{\mathrm{A}}$ the strength of the magnetic moment is increased by 0.1 to 0.4.

As discussed above, the exciton g factors are also sensitive to the region around K. In all cases we find that the difference of the magnetic moments decreases away from K and thus the g factors are clearly smaller compared to the interband values g_{band} at the K point. For the Mo-based TMDCs we find g^{A} ranges between −3.1 and −3.4, while WS_2 and WSe_2 have values of −2.8 and −3.0, respectively. For the different materials the trends of the g factors follow the trends described for g_{band} for both the A and B exciton. The reduction of the exciton g factor compared to g_{band} is slightly stronger in Mo-based TMDCs and is approximately 30%.

We note in passing that employing quasiparticle energies in Eq. (5) leads to g factors that are slightly larger by about 0.2, i.e., $g^{\mathrm{A}} = -3.2$, −3.4, −3.6, −3.0, and −3.3, respectively, for the materials listed in Table I.

Several experimental studies on exciton g factors have been performed in TMDC monolayers and their results are

listed in Table I. In general the data is quite scattered and values between −1.6 and −4.6 are observed for the A excitons. E.g., for $MoSe_2$ six measurements are available which range between −3.8 and −4.4. All in all, a one to one comparison of our results to experiment is not easily possible. Within measurements from the same groups (e.g., [10,12]) one can observe a weak tendency that W-based TMDC have smaller values compared to Mo based. If we compare g_{band} to experiment, one seems to find a very reasonable agreement. The decrease of about 30% of the exciton g factors results in generally slightly smaller values compared to the experiment. However, we note that experiments are not performed for freestanding monolayers. Additional dielectric screening (e.g., of the substrate) results in a weakening of the exciton binding energy, a larger spatial extent of the exciton, a smaller extent in $\mathbf{k}$ space [64], and eventually in larger exciton g factors. For hexagonal boron nitride substrate and encapsulation, e.g., the g factor increases by about 0.1 and 0.2. We believe that the dependence of the g factor on the environment might partially explain the scattering of experiments in Table I.

Furthermore, g factors for higher excited Rydberg excitons ($2s$ etc.) have been measured [11–13]. In most cases the g factors of $2s$ excitons increase compared to $1s$. As the spatial extent of these ns excitons increases with n, i.e., their extent in $\mathbf{k}$ space decreases [65]. This is perfectly in line with our results discussed above.

Conclusion.—In summary, we have proposed an approach to calculate magnetic moments and exciton g factors of semiconductors from first principles. Excluding excitonic effects, we obtain g_{band} factors ranging between −3.5 and −4.9 for monolayer WS_2 to $MoTe_2$, respectively. Employing $GW + \mathrm{BSE}$ calculations we find a distinct reduction of about 30% resulting in g factors which range between −2.8 and −3.4 for the excitons. Compared to the experimental results, our calculated values and trends are in good agreement and open a pathway for better understanding the change of optical properties of semiconductors in magnetic fields.

We thank Ashish Arora for many constructive discussions and helpful comments. The authors gratefully acknowledge the financial support from German Research Foundation (DFG Project No. DE 2749/2-1), the Collaborative Research Center SFB 1083 (Project No. A13), and the funding of computing time provided by the Paderborn Center for Parallel Computing (PC2).

Note added.—Recently, we became aware of that calculations of g_{band} for TMDCs have recently been posted in [66–68].

*thorsten.deilmann@wwu.de

[1] J. A. Wilson and A. D. Yoffe, The transition metal dichalcogenides discussion and interpretation of the observed optical, electrical and structural properties, Adv. Phys. **18**, 193 (1969).

[2] Y. Yafet, g factors and spin-lattice relaxation of conduction electrons, in *Solid State Physics* (Elsevier, New York, 1963), Vol. 14, pp. 1–98.

[3] M. Bayer, A. Kuther, A. Forchel, A. Gorbunov, V. B. Timofeev, F. Schäfer, J. P. Reithmaier, T. L. Reinecke, and S. N. Walck, Electron and Hole g Factors and Exchange Interaction from Studies of the Exciton Fine Structure in $In_{0.60}Ga_{0.40}As$ Quantum Dots, Phys. Rev. Lett. **82**, 1748 (1999).

[4] J. A. Gupta, D. D. Awschalom, X. Peng, and A. P. Alivisatos, Spin coherence in semiconductor quantum dots, Phys. Rev. B **59**, R10421(R) (1999).

[5] Y. Li, J. Ludwig, T. Low, A. Chernikov, X. Cui, G. Arefe, Y. D. Kim, A. M. van der Zande, A. Rigosi, H. M. Hill, S. H. Kim, J. Hone, Z. Li, D. Smirnov, and T. F. Heinz, Valley Splitting and Polarization by the Zeeman Effect in Monolayer $MoSe_2$, Phys. Rev. Lett. **113**, 266804 (2014).

[6] G. Aivazian, Z. Gong, A. M. Jones, R.-L. Chu, J. Yan, D. G. Mandrus, C. Zhang, D. Cobden, W. Yao, and X. Xu, Magnetic control of valley pseudospin in monolayer WSe_2, Nat. Phys. **11**, 148 (2015).

[7] A. Srivastava, M. Sidler, A. V. Allain, D. S. Lembke, A. Kis, and A. Imamoğlu, Valley Zeeman effect in elementary optical excitations of monolayer WSe_2, Nat. Phys. **11**, 141 (2015).

[8] A. Arora, R. Schmidt, R. Schneider, M. R. Molas, I. Breslavetz, M. Potemski, and R. Bratschitsch, Valley Zeeman splitting and valley polarization of neutral and charged excitons in monolayer $MoTe_2$ at high magnetic fields, Nano Lett. **16**, 3624 (2016).

[9] A. Arora, M. Drppel, R. Schmidt, T. Deilmann, R. Schneider, M. R. Molas, P. Marauhn, M. Potemski, M. Rohlfing, and R. Bratschitsch, Interlayer excitons in a bulk van der Waals semiconductor, Nat. Commun. **8**, 639 (2017).

[10] M. Koperski, M. R Molas, A. Arora, K. Nogajewski, M. Bartos, J. Wyzula, D. Vaclavkova, P. Kossacki, and M. Potemski, Orbital, spin and valley contributions to Zeeman splitting of excitonic resonances in $MoSe_2$, WSe_2 and WS_2 Monolayers, 2D Mater. **6**, 015001 (2018).

[11] S.-Y. Chen, Z. Lu, T. Goldstein, J. Tong, A. Chaves, J. Kunstmann, L. S. R. Cavalcante, T. Woniak, G. Seifert, D. R. Reichman *et al.*, Luminescent emission of excited Rydberg excitons from monolayer WSe_2, Nano Lett. **19**, 2464 (2019).

[12] M. Goryca, J. Li, A. V. Stier, T. Taniguchi, K. Watanabe, E. Courtade, S. Shree, C. Robert, B. Urbaszek, X. Marie *et al.*, Revealing exciton masses and dielectric properties of monolayer semiconductors with high magnetic fields, Nat. Commun. **10**, 4172 (2019).

[13] E. Liu, J. van Baren, T. Taniguchi, K. Watanabe, Y.-C. Chang, and C. H. Lui, Magnetophotoluminescence of exciton Rydberg states in monolayer WSe_2, Phys. Rev. B **99**, 205420 (2019).

[14] Z. Wang, K. F. Mak, and J. Shan, Strongly Interaction-Enhanced Valley Magnetic Response in Monolayer WSe_2, Phys. Rev. Lett. **120**, 066402 (2018).

[15] E. Liu, J. van Baren, T. Taniguchi, K. Watanabe, Y.-C. Chang, and C. H. Lui, Landau-Quantized Excitonic Absorption and

Luminescence in a Monolayer Valley Semiconductor, Phys. Rev. Lett. **124**, 097401 (2020).
[16] W. Kohn, Theory of Bloch electrons in a magnetic field: The effective Hamiltonian, Phys. Rev. **115**, 1460 (1959).
[17] L. M. Roth, Theory of Bloch electrons in a magnetic field, J. Phys. Chem. Solids **23**, 433 (1962).
[18] M.-C. Chang and Q. Niu, Berry phase, hyperorbits, and the Hofstadter spectrum: Semiclassical dynamics in magnetic Bloch bands, Phys. Rev. B **53**, 7010 (1996).
[19] D. Xiao, J. Shi, and Q. Niu, Berry Phase Correction to Electron Density of States in Solids, Phys. Rev. Lett. **95**, 137204 (2005).
[20] T. Thonhauser, D. Ceresoli, D. Vanderbilt, and R. Resta, Orbital Magnetization in Periodic Insulators, Phys. Rev. Lett. **95**, 137205 (2005).
[21] D. Xiao, M.-C. Chang, and Q. Niu, Berry phase effects on electronic properties, Rev. Mod. Phys. **82**, 1959 (2010).
[22] J.-P. Hanke, F. Freimuth, A. K. Nandy, H. Zhang, S. Blügel, and Y. Mokrousov, Role of Berry phase theory for describing orbital magnetism: From magnetic heterostructures to topological orbital ferromagnets, Phys. Rev. B **94**, 121114(R) (2016).
[23] M. Willatzen and L. C. L. Y. Voon, *The kp Method* (Springer, Berlin, Heidelberg, 2009).
[24] L. M. Roth, B. Lax, and S. Zwerdling, Theory of optical magneto-absorption effects in semiconductors, Phys. Rev. **114**, 90 (1959).
[25] C. E. Pryor and M. E. Flatté, Landé g Factors and Orbital Momentum Quenching in Semiconductor Quantum Dots, Phys. Rev. Lett. **96**, 026804 (2006).
[26] A. Kormnyos, P. Rakyta, and G. Burkard, Landau levels and Shubnikovde Haas oscillations in monolayer transition metal dichalcogenide semiconductors, New J. Phys. **17**, 103006 (2015).
[27] A. Arora, M. Koperski, A. Slobodeniuk, K. Nogajewski, R. Schmidt, R. Schneider, M. R. Molas, S. M. de Vasconcellos, R. Bratschitsch, and M. Potemski, Zeeman spectroscopy of excitons and hybridization of electronic states in few-layer WSe_2, $MoSe_2$ and $MoTe_2$, 2D Mater. **6**, 015010 (2018).
[28] M. Bieniek, M. Korkusiński, L. Szulakowska, P. Potasz, I. Ozfidan, and P. Hawrylak, Band nesting, massive Dirac fermions, and valley Landé and Zeeman effects in transition metal dichalcogenides: A tight-binding model, Phys. Rev. B **97**, 085153 (2018).
[29] D. V. Rybkovskiy, I. C. Gerber, and M. V. Durnev, Atomically inspired kp approach and valley Zeeman effect in transition metal dichalcogenide monolayers, Phys. Rev. B **95**, 155406 (2017).
[30] H. Rostami and R. Asgari, Valley Zeeman effect and spin-valley polarized conductance in monolayer MoS2 in a perpendicular magnetic field, Phys. Rev. B **91**, 075433 (2015).
[31] M. Rohlfing and S. G. Louie, Electron-hole excitations and optical spectra from first principles, Phys. Rev. B **62**, 4927 (2000).
[32] G. Onida, L. Reining, and A. Rubio, Electronic excitations: Density-functional versus many-body Green's-function approaches, Rev. Mod. Phys. **74**, 601 (2002).
[33] P. Ferriani, S. Heinze, G. Bihlmayer, and S. Blügel, Unexpected trend of magnetic order of 3d transition-metal monolayers on W(001), Phys. Rev. B **72**, 024452 (2005).
[34] J. Wieferink, P. Krüger, and J. Pollmann, Improved Hybrid Algorithm with Gaussian Basis Sets and Plane Waves: First-Principles Calculations of Ethylene Adsorption on β-SiC (001) - (3×2), Phys. Rev. B **74**, 205311 (2006).
[35] See Supplemental Material at http://link.aps.org/supplemental/10.1103/PhysRevLett.124.226402 for details of the theoretical method, its convergence, and the Berry curvature, which includes additional Refs. [36–44].
[36] J. P. Perdew and A. Zunger, Self-interaction correction to density-functional approximations for many-electron systems, Phys. Rev. B **23**, 5048 (1981).
[37] D. R. Hamann, Generalized norm-conserving pseudopotentials, Phys. Rev. B **40**, 2980 (1989).
[38] L. Kleinman and D. M. Bylander, Efficacious Form for Model Pseudopotentials, Phys. Rev. Lett. **48**, 1425 (1982).
[39] L. A. Hemstreet, C. Y. Fong, and J. S. Nelson, First-principles calculations of spin-orbit splittings in solids using nonlocal separable pseudopotentials, Phys. Rev. B **47**, 4238 (1993).
[40] B. Stärk, P. Krüger, and J. Pollmann, Magnetic anisotropy of thin Co and Ni films on diamond surfaces, Phys. Rev. B **84**, 195316 (2011).
[41] M. Rohlfing, Electronic excitations from a perturbative LDA + GdW approach, Phys. Rev. B **82**, 205127 (2010).
[42] N. Sai, K. M. Rabe, and D. Vanderbilt, Theory of structural response to macroscopic electric fields in ferroelectric systems, Phys. Rev. B **66**, 104108 (2002).
[43] W. Feng, Y. Yao, W. Zhu, J. Zhou, W. Yao, and D. Xiao, Intrinsic spin hall effect in monolayers of group-vi dichalcogenides: A first-principles study, Phys. Rev. B **86**, 165108 (2012).
[44] T. P. Lyons, S. Dufferwiel, M. Brooks, F. Withers, T. Taniguchi, K. Watanabe, K. S. Novoselov, G. Burkard, and A. I. Tartakovskii, The valley Zeeman effect in inter- and intra-valley trions in monolayer WSe_2, Nat. Commun. **10**, 2330 (2019).
[45] C. J. Pickard and M. C. Payne, Second-order kp perturbation theory with Vanderbilt pseudopotentials and plane waves, Phys. Rev. B **62**, 4383 (2000).
[46] T. Y. Kim, A. Ferretti, and C.-H. Park, Effects of spin-orbit coupling on the optical response of a material, Phys. Rev. B **98**, 245410 (2018).
[47] Z. H. Levine and D. C. Allan, Linear Optical Response in Silicon and Germanium Including Self-Energy Effects, Phys. Rev. Lett. **63**, 1719 (1989).
[48] L. Hedin, New method for calculating the one-particle Green's function with application to the electron-gas problem, Phys. Rev. **139**, A796 (1965).
[49] M. Drüppel, T. Deilmann, J. Noky, P. Marauhn, P. Krüger, and M. Rohlfing, Electronic excitations in transition metal dichalcogenide monolayers from an LDA + GdW approach, Phys. Rev. B **98**, 155433 (2018).
[50] G. Sundaram and Q. Niu, Wave-packet dynamics in slowly perturbed crystals: Gradient corrections and Berry-phase effects, Phys. Rev. B **59**, 14915 (1999).
[51] F. Cadiz, E. Courtade, C. Robert, G. Wang, Y. Shen, H. Cai, T. Taniguchi, K. Watanabe, H. Carrere, D. Lagarde, M. Manca, T. Amand, P. Renucci, S. Tongay, X. Marie, and B. Urbaszek, Excitonic Linewidth Approaching the Homogeneous Limit in MoS_2-Based van der Waals Heterostructures, Phys. Rev. X **7**, 021026 (2017).

[52] A. V. Stier, K. M. McCreary, B. T. Jonker, J. Kono, and S. A. Crooker, Exciton diamagnetic shifts and valley Zeeman effects in monolayer WS_2 and MoS_2 to 65 Tesla, Nat. Commun. **7**, 10643 (2016).

[53] A. A. Mitioglu, K. Galkowski, A. Surrente, L. Klopotowski, D. Dumcenco, A. Kis, D. K. Maude, and P. Plochocka, Magnetoexcitons in large area CVD-grown monolayer MoS_2 and $MoSe_2$ on sapphire, Phys. Rev. B **93**, 165412 (2016).

[54] D. MacNeill, C. Heikes, K. F. Mak, Z. Anderson, A. Kormanyos, V. Zolyomi, J. Park, and D. C. Ralph, Breaking of Valley Degeneracy by Magnetic Field in Monolayer $MoSe_2$, Phys. Rev. Lett. **114**, 037401 (2015).

[55] G Wang, L Bouet, M M Glazov, T Amand, E L Ivchenko, E Palleau, X Marie, and B Urbaszek, Magneto-optics in transition metal diselenide monolayers, 2D Mater. **2**, 034002 (2015).

[56] G. Plechinger, P. Nagler, A. Arora, A. G. del Águila, M. V. Ballottin, T. Frank, P. Steinleitner, M. Gmitra, J. Fabian, P. C. M. Christianen *et al.*, Excitonic valley effects in monolayer WS_2 under high magnetic fields, Nano Lett. **16**, 7899 (2016).

[57] J. Zipfel, J. Holler, A. A. Mitioglu, M. V. Ballottin, P. Nagler, A. V. Stier, T. Taniguchi, K. Watanabe, S. A. Crooker, P. C. M. Christianen, T. Korn, and A. Chernikov, Spatial extent of the excited exciton states in WS_2 monolayers from diamagnetic shifts, Phys. Rev. B **98**, 075438 (2018).

[58] M. Koperski, K. Nogajewski, A. Arora, V. Cherkez, P. Mallet, J.-Y. Veuillen, J. Marcus, P. Kossacki, and M. Potemski, Single photon emitters in exfoliated WSe_2 structures, Nat. Nanotechnol. **10**, 503 (2015).

[59] S. Haastrup, M. Strange, M. Pandey, T. Deilmann, P. S. Schmidt, N. F. Hinsche, M. N. Gjerding, D. Torelli, P. M. Larsen, A. C. Riis-Jensen, J. Gath, K. W. Jacobsen, J. J. Mortensen, T. Olsen, and K. S. Thygesen, The computational 2D materials database: High-throughput modeling and discovery of atomically thin crystals, 2D Mater. **5**, 042002 (2018).

[60] G. Strinati, Dynamical Shift and Broadening of Core Excitons in Semiconductors, Phys. Rev. Lett. **49**, 1519 (1982).

[61] G. Wang, C. Robert, M. M. Glazov, F. Cadiz, E. Courtade, T. Amand, D. Lagarde, T. Taniguchi, K. Watanabe, B. Urbaszek, and X. Marie, In-Plane Propagation of Light in Transition Metal Dichalcogenide Monolayers: Optical Selection Rules, Phys. Rev. Lett. **119**, 047401 (2017).

[62] T. Deilmann and K. S. Thygesen, Dark excitations in monolayer transition metal dichalcogenides, Phys. Rev. B **96**, 201113(R) (2017).

[63] T. Deilmann and K. S. Thygesen, Finite-momentum exciton landscape in mono- and bilayer transition metal dichalcogenides, 2D Mater. **6**, 035003 (2019).

[64] M. Drüppel, T. Deilmann, P. Krüger, and M. Rohlfing, Diversity of trion states and substrate effects in the optical properties of an MoS_2 monolayer, Nat. Commun. **8**, 2117 (2017).

[65] D. Y. Qiu, F. H. da Jornada, and S. G. Louie, Screening and many-body effects in two-dimensional crystals: Monolayer MoS_2, Phys. Rev. B **93**, 235435 (2016).

[66] T. Woźniak, P. E. F. Junior, G. Seifert, A. Chaves, and J. Kunstmann, Exciton g-factors of van der Waals heterostructures from first principles calculations, arXiv:2002.02542.

[67] J. Förste, N. V. Tepliakov, S. Y. Kruchinin, J. Lindlau, V. Funk, M. Förg, K. Watanabe, T. Taniguchi, A. S. Baimuratov, and A. Högele, Exciton g-factors in monolayer and bilayer WSe_2 from experiment and theory, arXiv:2002.11646.

[68] F. Xuan and S. Y. Quek, Valley Zeeman effect and Landau levels in two-dimensional transition metal dichalcogenides, arXiv:2002.11993.